Atmos. Meas. Tech. Discuss., 7, 8067–8100, 2014
www.atmos-meas-tech-discuss.net/7/8067/2014/
doi:10.5194/amtd-7-8067-2014

Atmospheric Measurement Techniques Discussions

Accurate laser measurements of ozone absorption cross-sections in the Hartley band

J. Viallon[1], S. Lee[2], P. Moussay[1], K. Tworek[3], M. Petersen[4], and R. I. Wielgosz[1]

[1]Bureau International des Poids et Mesures (BIPM), Sèvres, France
[2]Korean Research Institute of Standards and Science (KRISS), Daejeon, Republic of Korea
[3]Central Office of Measures (GUM), Warsaw, Poland
[4]University of Neuchâtel, Switzerland

Received: 13 May 2014 – Accepted: 17 July 2014 – Published: 5 August 2014

Correspondence to: J. Viallon (jviallon@bipm.org)

Published by Copernicus Publications on behalf of the European Geosciences Union.

Abstract

Ozone plays a crucial role in tropospheric chemistry, is the third largest contributor to greenhouse radiative forcing after carbon dioxide and methane and also a toxic air pollutant affecting human health and agriculture. Long-term measurements of tropospheric ozone have been performed globally for more than 30 years with UV photometers, all relying on the absorption of ozone at the 253.65 nm line of mercury. We have re-determined this cross-section and report a value of 11.27×10^{-18} cm^2 molecule^{-1} with an expanded relative uncertainty of 0.84 %. This is lower than the conventional value currently in use and measured by Hearn in 1961 with a relative difference of 1.8 %, with the consequence that historically reported ozone concentrations should be increased by 1.8 %. In order to perform the new measurements of cross sections with reduced uncertainties, a system to generate pure ozone in the gas phase together with an optical system based on a UV laser with lines in the Hartley band, including accurate path length measurement of the absorption cell and a careful evaluation of possible impurities in the ozone sample by mass spectrometry and Fourier Transform Infrared spectroscopy was setup. This resulted in new measurements of absolute values of ozone absorption cross sections of 9.48×10^{-18}, 10.44×10^{-18}, and 11.07×10^{-18} cm^2 molecule^{-1}, with relative expanded uncertainties better than 0.6 %, for the wavelengths (in vacuum) of 244.062, 248.32, and 257.34 nm respectively. The cross-section at the 253.65 nm line of mercury was determined by comparisons using a Standard Reference Photometer equipped with a mercury lamp as the light source. The newly reported value should be used in the future to obtain the most accurate measurements of ozone concentration, which are in closer agreement with non UV photometry based methods such as the gas phase titration of ozone with nitrogen monoxide.

AMTD
7, 8067–8100, 2014

1 Introduction and aims

The property of ozone to strongly absorb UV radiation, notably in the Hartley Band, and the relative ease of reproducing a mercury line at 253.65 nm (in air) has led to the value of the ozone absorption cross section at this wavelength becoming particularly important for global ozone atmospheric monitoring. Efforts to improve its accuracy continue, as reviewed (Orphal, 2002), because it directly impacts on all results from instruments based on UV absorption. This is the case in a majority of surface ozone measurements, for which an ISO method has been developed (ISO, 1996). The National Institute for Science and Technology (NIST) Standard Reference Photometer (SRP), operates on this principal, and also acts as the primary standard for numerous national and international ozone monitoring networks, such as the WMO Global Atmosphere Watch (GAW) Programme (Galbally et al., 2013; Klausen et al., 2003). Several replicas of this instrument are maintained by the International Bureau of Weights and Measures (BIPM), one of which is the reference for international comparisons of national ozone standards coordinated by the BIPM. The ozone absorption cross-section value at the 253.65 nm wavelength (Hearn, 1961) is the measured value used in the SRP, and was adopted as a conventional value during the Quadriennal Ozone Symposium in 1984 together with measurements by Bass and Paur for other wavelengths (Bass and Paur, 1984). Measurements of ozone absorption at other wavelengths have often been scaled to the value at 253.65 nm, since they were performed in ozone in air mixture, of which the ozone concentration is determined using its absorption at this wavelength. Broadband cross-section measurements with improved spectral resolution as well as an extended temperature range are required to match the conditions expected during atmospheric observations, such as those reported in a recent study (Serdyuchenko et al., 2014; Gorshelev et al., 2014) performed at IUP-Bremen. However, as highlighted by the authors, technical choices that are inherent to broadband laboratory measurements impose a limitation on achievable uncertainties to around 2–3 % of the cross-section value.

AMTD
7, 8067–8100, 2014

Measurements performed at selected wavelengths and at room temperature can be performed with lower uncertainty than broadband measurements. This is mainly due to the use of a monochromatic light source, usually a mercury lamp, with well-defined wavelength(s). In addition, by limiting measurements to the strongest absorbing region of the spectrum, close to 255 nm, all measurements can be performed with a single absorption cell, over a limited ozone pressure range and in a limited time to avoid ozone decay due to dissociation, as reported (Mauersberger et al., 1985, 1986, 1987), with two reported values of the cross-section having a small relative standard uncertainty (0.5 and 0.7 %), and biased by 0.8 and 1.4 % from the 1961 value reported by Hearn.

During the first international comparison of ozone standards for ground level ozone conducted by the BIPM, twenty three laboratories reported results based on UV absorption compared to two laboratories reporting ozone concentration measurements based on gas phase titration systems: the National Institute for Environmental Studies of Japan as described by Tanimoto et al. (2006) and the BIPM (Viallon et al., 2006a). Gas phase titration involves reacting ozone in air with nitrogen monoxide, and measuring either the loss of nitrogen monoxide or the gain of the reaction product, nitrogen dioxide, to deduce the ozone concentration in the sample. The 2 to 3 % bias observed between the methods (gas phase titration reporting higher ozone concentrations) could be explained by a biased ozone absorption cross-section value, which represents the major uncertainty component in measurements based on UV photometry.

In 2007, the BIPM started a laboratory programme to perform new measurements of the ozone absorption cross-section with improved accuracy. Efforts focused on two major sources of uncertainty in the measurements: ozone purity and knowledge of the light path length. The BIPM first developed a laser ozone photometer, capable of measuring ozone concentrations in the same range as the SRP but with improved accuracy, as described in Petersen et al. (2012). This instrument was used to deduce new values of the ozone cross-section in the Hartley band, relative to the reference value obtained by Hearn at 253.65 nm.

AMTD
7, 8067–8100, 2014

In the present study, absolute measurements of the ozone cross-section at the same wavelengths have been determined with the smallest uncertainties published to date. This required a cryogenic ozone generator to be developed, together with a method based on cycles of evaporation-condensation of ozone so as to better evaluate the purity of gaseous samples on which UV absorption measurements were performed. The measurement setup and associated process are first presented in Sect. 2, which includes additional purity analyses by mass spectrometry and Fourier Transform Infrared spectroscopy (FTIR). The motivation for this work was to obtain a reduction in uncertainties and all possible sources of uncertainty are considered and evaluated in Sect. 3. Finally, values of the ozone cross-sections are presented in comparison with previous studies in Sect. 4 and a new value at the reference wavelength of 253.65 nm is calculated in Sect. 5. This work is in agreement with recent measurement results that indicate that the historical conventional cross-section value used for surface ozone measurements is biased too high, resulting in an underestimation of ozone concentrations, which can be corrected by use of the value published in this work.

2 Measurement setup and process

The setup, shown in Fig. 1, consists of four major parts: a silent discharge cryogenic ozone generator (CRYO), an absorption cell (AC), a pressure gauge (CDG) and a quadrupole mass spectrometer (RGA). The discharge cryogenic ozone generator is where ozone was generated from an electric discharge in pure oxygen (Linde, grade 6.0), using a method similar to that described by Janssen et al. (2011). The absorption cell is made of quartz and is where gaseous ozone at room temperature was introduced to allow absorption measurements to be performed with an intensity stabilized UV laser beam. The pressure gauge is a capacitive diaphragm gauge with its heater turned off (1 Torr MKS 690A Baratron coupled with a MKS 670B signal conditioner) and is used to monitor the pressure of ozone samples at room temperature as well as the pressure of residual gases when ozone was condensed in the cryostat. The

AMTD
7, 8067–8100, 2014

quadrupole mass spectrometer (RGA model MKS Vision 1000 C) is used to check the composition of residual gases. An additional pressure gauge (Pirani, Pfeiffer vacuum MPT100 / PTR35-130) was used to monitor the oxygen pressure during ozone generation and the vacuum pressure during evacuation of gases with a turbo-molecular pump (TMP – Edwards STP 301C backed up with a primary pump Edwards XDS 10). Except for the quartz absorption cell, the measurement volume, i.e. the volume closed by valves V1, V2, V3 and V4 is made of 316L stainless steel, including the 4 valves (VAT KE01) in which only the metal is in contact with the vacuum.

2.1 Ozone production and storage

Ozone was produced in a silent discharge cryogenic ozone generator especially designed for this purpose. The generation chamber is a long (~ 50 cm) double wall cylinder in quartz with a 3.9 mm gap width in which a glow discharge was created by applying a high voltage (20 kV, 20–70 kHz, typical current 1 mA) to two aluminium foils maintained on the inside and outside of the cylinder walls. Valves V2 and V3 are closed, oxygen grade 6.0, the purity of which was further checked using the RGA, was introduced at a pressure of about 55 mbar into the generator, valve V4 was closed and the high voltage turned on to produce the silent discharge. About 90 % of the 50 cm long cylinder was kept inside a liquid nitrogen variable temperature cryostat (Janis VNF-100, with an operating temperature range of 60 K to 325 K, and temperature stability of 50 mK). With this design, it was found that the efficiency of ozone generation was at a maximum when the cryostat was kept between 88 K and 92 K, as measured with an additional temperature probe placed on the bottom of the ozone generator, inside the cryostat. After two to three hours, a droplet of liquid ozone was observed on the bottom of the ozone generator, through the two quartz windows of the cryostat. The presence of liquid ozone meant that the silent discharge could then be turned off, and the cryostat temperature further reduced to 73 K, so as to trap all the ozone created inside the generator. Finally, the system was evacuated and the condensate was pumped for 20 min to remove oxygen and any other residual gases. The resulting amount of liquid ozone

AMTD
7, 8067–8100, 2014

was sufficient to start absorption measurements using evaporation-condensation cycles as described in Sect. 2.2, starting with a first cycle of longer duration (20 min) and at the maximum ozone pressure of 1 mbar to passivate all surfaces.

2.2 Ozone evaporation-condensation cycles

Using the liquid ozone trapped in the bottom of the ozone generator, a series of evaporation-condensation cycles was performed so as to obtain about 9 different ozone pressures in the gas cell to cover the range 0.2 mbar to 1 mbar, whilst measuring the absorbance A_e at a fixed laser wavelength to determine the ozone cross-section. The process followed during those cycles was optimized during extensive testing to maximize the purity of the gaseous ozone samples released into the gas cell. The key parameters to monitor were the cryostat temperature T_{cryo}, the sample total pressure P_T measured with the Baratron, and the ozone partial pressure $P(O_3)$ which at this point was used as an indicative real-time value determined using the following equation:

$$P(O_3) = \frac{A_e R T_{cell}}{\sigma N_A L_{opt}} \quad (1)$$

Where A_e is the absorbance, T_{cell} the gas cell temperature, N_A the Avogadro constant, R the gas constant and σ a value of the ozone cross-section chosen from the literature (the so-called BDM data set was used in this instance). These three parameters are displayed in Fig. 1 as recorded during the 15 min of a typical evaporation-condensation cycle. Each cycle started at time t with valves V1 and V3 closed and V2 and V4 open to evacuate the gas cell and record the light intensity under vacuum I. Then V2 was closed to prevent ozone entering the Baratron pressure gauge where it could start to dissociate. In order to avoid rapid dissociation, the pressure gauge was maintained at room temperature rather than being heated to its normal operating temperature of 45 °C. Meanwhile, V1 was opened to allow pumping of the condensate for 5 min to remove any residual impurity. At time $t = 5$ min, the cryostat target temperature was set to 105 K. At time $t = 6$ min, the valve V4 was closed to stop pumping, allowing the ozone

AMTD
7, 8067–8100, 2014

pressure to increase with the cryostat temperature. When $P(O_3)$ reached the target pressure (about 1 mbar in the figure), V1 was closed and the cryostat target temperature set to 73 K, which was reached in less than one minute. At that time V2 was opened to start recording the total pressure in the gas cell for approximately 30 s. During post-treatment, the last values of the total pressure and of the light intensity recorded during this particular period were selected to further compute the cross-section. Then V1 was opened and all the gaseous ozone was condensed again, lowering the total pressure to the residual pressure P_{res}, of the order of 0.01 mbar. When this pressure was stable, V1 was closed and V3 opened to allow the analysis of residual gases with the RGA for typically one minute. Finally the absorption cell was fully evacuated down to 10^{-7} mbar to start a new evaporation-condensation cycle.

2.3 Optical setup for absorption measurements

The optical setup was the same as described in Petersen et al. (2012) for the laser ozone photometer, except that the measurement cell was a 5 cm long absorption cell (AC in Fig. 1) in quartz. The UV light was produced with an argon-ion laser doubled in frequency emitting light at either 244.06 nm, 248.32 nm or 257.34 nm (wavelengths in vacuum).

Light traps (LT1 and LT2) composed of 3 window-less Hamamatsu S1337-1010-N photodiodes were used for detection of the UV beam. A spatial filter composed of a 75 mm focal length lens and a 20 µm pinhole was used to give the beam a Gaussian shape. A 200 MHz acousto-optic modulator (AOM) for UV-light between 244 nm and 266 nm was used to stabilize the power-level of the light on the LT1 light trap. The light power density was typically less than 10 µW cm^{-2}, and it was previously verified in Petersen et al. (2012) that there were no significant non-linear effects at this level.

The 5 cm long cell is made of quartz with fused silica windows tilted at 3° to avoid multiple reflections of the beam inside the cell. The windows at each end of a cell are tilted in the same direction to maintain the same cell length. To ensure a consistent beam alignment through the cells, diaphragms were mounted before and after the cell

AMTD
7, 8067–8100, 2014

in fixed positions and opened to less than 3 mm in diameter. The light path length was measured before and after the ozone absorption measurement by interferometry, following a method described in Sect. 2.3.1. To remove air turbulence and to significantly reduce temperature changes and background lighting the entire optical setup was enclosed in a thin aluminium casing and the cell in a thin black Plexiglas.

2.3.1 Absorption cell length measurements

The method used for measuring the absorption cell length is based on counting interference fringes produced in a Michelson interferometer with the absorption cell placed in one of its arms, when evacuating the cell from air at ambient pressure to vacuum, due to the varying index of refraction in the arm with the cell. This method follows the process described in Castrillo et al. (2003) which accurately measures the light path length in a CO_2 absorption cell. The interferometer was setup to have two parallel arms, with the light travelling through the room air in one arm and through the absorption cell in the other arm. A 5 mW He-Ne laser emitting light at 633.991 nm was used as the light source and its wavelength was accurately measured with the wavemeter. The ambient air pressure present in the absorption cell before pumping was measured with a barometer (Paroscientific model 740) traceable to the BIPM Mass Department. The vacuum pressure was measured with the Baratron. A dosing valve was used to limit the speed of the pressure drop during pumping. In a typical measurement, starting from an air pressure of 1018.84 hPa and ending with less than 0.2 hPa, 41.35 fringes were counted, resulting in a path length of 48.32 mm with a standard uncertainty of 0.06 mm (at 65 % degree of confidence or 1 σ), according to the equation:

$$(n-1)L_{\mathrm{opt}} = \frac{F\lambda_{\mathrm{a}}}{2} \tag{2}$$

Where n is the index of refraction of air given by Edléns updated formula (Birch and Downs, 1993), L_{opt} is the light path length in the absorption cell, F is the number of fringes and λ_{a} is the laser wavelength in air.

AMTD
7, 8067–8100, 2014

A series of twenty repeat measurements resulted in an average path length of 48.33 mm, which was consistent with measurements of the cell length using a coordinate machine, which gave a value of 48.35 mm.

2.4 Ozone purity

The purity of the ozone sample is of primary importance when measuring accurate ozone cross-sections. A careful analysis of the uncertainties shows that any impurity that would be above 1 % in the sample should be measured and taken into account if the target uncertainty of the ozone cross-section is to be below 1 %. It is well known that, even when starting measurements with pure ozone samples, dissociation of ozone following collisions and interactions with surfaces will lead to the formation of oxygen. In addition, leaks within the system and reaction of ozone with contaminated surfaces could potentially lead to other trace contaminants being present. A comprehensive study of possible contaminants in ozone samples generated from oxygen by discharges followed by cryogenic distillation was performed by Janssen et al. (2011). As expected, oxygen was found to be the major impurity with a mole fraction of 1 mmol mol^{-1}, followed by nitrous oxide at 0.3 mmol mol^{-1}.

The setup adopted in this work was similar to that selected by Janssen, except that the chosen evaporation temperature for ozone was set to 105 K. This has the advantage of ensuring that potential impurities such as carbon dioxide, nitrous oxide and water remain in the liquid phase. The only impurity that needs to be considered in this case is oxygen, and in a first approach the ozone purity could be deduced from pressure and absorption measurements only, as presented below.

For a given evaporation-condensation cycle, the ozone mole fraction was deduced from the difference between the total pressure measured just before condensation P_T and the residual pressure when ozone was condensed P_{res}. The residual pressure was corrected for the ozone pressure, determined using Eq. (1), which is of the order of

AMTD
7, 8067–8100, 2014

0.003 mbar at the temperature of the cryostat (close to 73 K):

$$x(O_3) = 1 - \frac{P_{res} - P_{vap}(O_3)}{P_T} \quad (3)$$

During the nine series of measurements performed, the residual gas pressure was typically between 0.005 mbar and 0.01 mbar, mainly depending on the sample pressure before condensation. The ozone vapour pressure had a mean value of 3.47×10^{-3} mbar with a standard deviation of 0.5×10^{-3} mbar. The same value was found regardless the laser wavelength, giving more confidence in the robustness of this measurement. In order to verify that the oxygen formed from ozone decomposition was well mixed within the ozone, the variation of the total pressure ΔP_T measured while the Baratron gauge was in contact with the ozone sample was always compared with the variation of the ozone partial pressure $\Delta P(O_3)$, determined from absorption measurements. Typical values were ΔP_T between 5×10^{-4} mbar and 10^{-3} mbar and half the value of $-\Delta P(O_3)$, as expected if ozone decomposes to only oxygen and is well mixed.

The ozone mole fraction in the "pure" ozone sample calculated for all measurement points is plotted in Fig. 3 vs. the sample pressure before condensation. It shows minimum values of 0.989 mol mol^{-1}, and maximum values of 0.998 mol mol^{-1}. Therefore, in most cases the amount of impurities could be considered negligible, but nevertheless should be accounted for in calculated measurement uncertainties.

Although the above results already demonstrate a good purity level of ozone, two complementary techniques were implemented for validation of the impurity levels: Residual Gas Analysis (RGA) by Mass Spectrometry and Fourier Transformed Infrared spectroscopy (FTIR). The RGA was mainly used to analyse the residuals gases, whereas FTIR was used for a direct analysis of infrared active molecules in the gaseous ozone samples. Both measurements are described below.

AMTD
7, 8067–8100, 2014

2.4.1 Analysis of residual gases by mass spectrometry

Mass spectrometry has already been used to analyse impurities in ozone samples by Anderson and Mauersberger (1981), Mauersberger et al. (1986, 1985). It is however a complex measurement, as the ozone molecule is fragmented due to the impact of the electron beam required to produce ions, in addition to the possible dissociation due to non-polished metallic surfaces or even the presence of polymers within many commercially available mass spectrometers. The RGA used in the facility contains some non-metallic parts and not all of them could be replaced, resulting in rapid dissociation of ozone into molecular oxygen whenever the valve V3 to the RGA was opened, resulting in an inability to make accurate measurements of oxygen impurities in gaseous ozone. However, the RGA is a suitable instrument for residual gas analysis and could be meaningfully used to record mass spectra of the residual gases. For each evaporation-condensation cycle, one mass spectrum of the ozone vapour was recorded just before the cycle started, after having pumped on liquid ozone maintained at 73 K. Then a second mass spectrum was recorded when the cycle was completed, when the ozone was again condensed at 73 K. In general the intensity at mass 32 is partly due to the presence of molecular oxygen, and partly due to the fragmentation of ozone within the entrance of the RGA instrument where molecules entering collide with the electron beam. The difference ΔI_{32} between the signal at mass 32 recorded on the residual gases after condensation and on the ozone vapour can be attributed to molecular oxygen resulting from the dissociation of ozone during the evaporation cycle,. A quantitative analysis was further performed, computing the oxygen pressure resulting from dissociation during the evaporation from ΔI_{32}. After each series of measurement, the signal intensity at mass 32 I_{32} was calibrated using pure oxygen at three different pressures covering the same range, typically between 0.001 mbar and 0.01 mbar.

The results of the two available methods to deduce the oxygen pressure in the residuals is shown in Fig. 4 against the sample pressure during the evaporation phase: with

AMTD
7, 8067–8100, 2014

squares (a) for the oxygen pressure deduced from the difference $P_{res} - P_{vap}(O_3)$ between the residual pressure and the ozone vapour pressure, and with circles (b) for the oxygen pressure deduced from the difference in the RGA signal at mass 32, after calibration of the RGA with pure oxygen. Figure 4 shows good agreement between both methods, within their uncertainties, confirming that oxygen could be considered as the main component of the residual gas.

2.4.2 Analysis of samples by FTIR

The above measurements with the RGA provide an analysis of the residual gases after condensation of the ozone sample. It could be argued that some compounds could always be evaporated and condensed simultaneously with ozone, and thus not detected by the RGA. This could happen for example if the evaporation temperature of 105 K, measured at the bottom of the cryostat, is maintained only in this part, while the upper part remains at a higher temperature allowing the carbon dioxide trapped in the solid form to sublime.

In order to further confirm the absence of carbon dioxide, it was decided to perform an FTIR analysis of the gaseous ozone sample. A gas cell with a short path length of 10 cm was installed in a FTIR (ThermoScientific Nicolet Nexus) spectrometer configured with a mercury cadmium telluride (MCT) high D* liquid N_2-cooled mid-infrared detector. The resolution had to be degraded to 4 cm^{-1} to compensate for the low signal to-noise ratio reached at these low pressures and to obtain a better signal in the carbon dioxide absorption band (2300 cm^{-1} to 2400 cm^{-1}). The FTIR gas cell was linked to the ozone generator using about one metre of stainless tubing due to the size of the spectrometer. Nothing else was modified in the setup described previously. A difficulty arising from this setup is the rapid reaction of ozone in contact with metallic surfaces and the few O-rings in the connections to the FTIR cell, leading to a rapid increase of the carbon dioxide signal. The measurement process was improved by several hours of passivation at high ozone pressure (about 9 mbar) and several cycles of filling both the UV absorption cell and the FTIR cell with ozone and then pumping down to 10^{-7} mbar.

AMTD
7, 8067–8100, 2014

By doing so, the same process as used during the cross-section measurement to evaporate at least 1 mbar of ozone in the cell could be reproduced, resulting in FTIR spectra in which the carbon dioxide signal became undetectable. An example is displayed in Fig. 5 with a spectrum recorded on gaseous ozone at 3 mbar, in which the carbon dioxide signal is barely visible. In contrast, the signal recorded after 12 h with the same sample in the system clearly shows an increase of carbon dioxide and a decrease of ozone, certainly due to reaction with surfaces.

In a second step, FTIR spectra were recorded on pure carbon dioxide at known pressure (measured with the Baratron) and this showed that a pressure as low as 10^{-3} mbar of CO_2 could be detected with this experimental setup. As no CO_2 could be detected on samples of ozone at 1 mbar, it was concluded that carbon dioxide was absent from the gaseous ozone samples, within the limit of detection of the FTIR for CO_2, taken as three times 10^{-3} mbar.

3 Measurement equation and uncertainties

The ozone absorption cross-section can be deduced for a given ozone sample from the Beer-Lambert law:

$$\sigma = \frac{R A_e T_{cell}}{N_A L_{opt} x(O_3) P_T} \quad (4)$$

Where $A_e = -\ln(I/I_0)$ is the absorbance measured in real-time in the absorption cell, P_T the total pressure and $x(O_3)$ is the ozone mole fraction in the sample.

In practice all parameters were recorded for each of the nine evaporation-condensation cycles performed during a series of measurements, and a linear fit was performed to deduce the ozone cross-section associated with each series. Three repeated series were recorded for each wavelength, and the average cross-section was further calculated.

AMTD
7, 8067–8100, 2014

All the uncertainties in this section are calculated according to the Guide for Uncertainties in Measurements (BIPM et al., 1995).

3.1 Pressure measurements

The pressure inside the gas cell was measured with the CDG described in Sect. 2 with its heater turned off. Pressure measurements were effectively performed in two distinct ranges of the pressure gauge: from 0.2 mbar to 1 mbar when the gauge was in contact with the gaseous ozone sample, and from 0.005 mbar to 0.015 mbar when it was employed to measure the pressure of the gas above liquid ozone, before or after an evaporation-condensation cycle. Furthermore, while the pressure above liquid ozone was a static measurement, the measurement performed on gaseous samples was a dynamic measurement due to the gauge being suddenly placed in contact with the gas, after being kept at about 0.001 mbar for several minutes, after which a rapid measurement was performed under a constantly increasing pressure due to the dissociation of ozone in oxygen. The pressure gauge was therefore calibrated in situ by comparison with another CDG (MKS model PR4000) itself regularly calibrated by the French national metrology institute LNE (Laboratoire National de Métrologie et d'Essais), using two different approaches to match the measurements in these two ranges.

In the range 0.005 mbar to 0.015 mbar, a static calibration was performed, introducing nitrogen at ten fixed pressure points in a closed part of the setup, and recording measurements when the desired stability (standard deviation lower than 10^{-5} mbar) was reached. Using this process the calibration uncertainty was dominant, leading to a standard uncertainty expressed in mbar of:

$$u_{\mathrm{cal}}(P) = 10^{-3}P + 5\times10^{-5} \quad (5)$$

In the range 0.1 mbar to 1 mbar a dynamic calibration was performed in addition to the static calibration. During the dynamic calibration, nitrogen was introduced at an appropriate flow rate to obtain a constantly increasing pressure with a rate increase

AMTD
7, 8067–8100, 2014

that matched the rate observed during measurements on ozone samples, typically of 5×10^{-3} mbar min^{-1}. Both dynamic and static calibrations agreed very well, resulting in the same calibration parameters. As the transfer standard PR4000 was calibrated in the low range 0.005 mbar to 0.1 mbar, a linear extrapolation was applied, followed by a correction as the sensor was used at room temperature instead of the recommended temperature of 45 °C, using the formula provided by Daudé et al. (2013). It was observed that this treatment obtained results that agreed with the results of a calibration of the same sensor performed at 45 °C one month previously by the LNE, confirming the validity of our in situ calibration process. Noting that the resolution and stability of the sensor are better than the calibration uncertainty, Eq. (5) was also used to calculate uncertainties associated with the ozone sample pressure measurements.

3.2 Ozone purity

The ozone purity was evaluated as the ozone mole fraction $x(O_3)$ expressed in mol mol^{-1} using Eq. (3). Its associated uncertainty is a combination of the residual pressure, sample pressure, and ozone vapour pressure uncertainties. The first two terms are explained in the previous section. The ozone vapour pressure was deduced from absorption measurements, using literature values from Brion, Daumont and Malicet (also called BDM values), (Brion et al., 1993, 1998; Malicet et al., 1995) for the ozone cross-section, with a standard uncertainty of 2 %. This uncertainty is sufficiently large to easily cover all probable values of the ozone cross section, and makes the result independent of the actual literature value used from among those published. Applying the uncertainty propagation law to Eq. (3), the combined standard uncertainty associated with the ozone mole fraction is between 5×10^{-4} mol mol^{-1} at low sample pressure and 10^{-4} mol mol^{-1} for the highest values of the sample pressure range.

This uncertainty was further combined with a component evaluated from the FTIR measurements of carbon dioxide, considering no carbon dioxide with flat uncertainty probability distribution between zero and 3×10^{-3} mbar, resulting in a standard

AMTD
7, 8067–8100, 2014

uncertainty of 2 mmol mol^{-1} which therefore dominates the uncertainty on the ozone mole fraction.

3.3 Ozone temperature

The temperature in the absorption cell was measured by a thermo-resistor of 1 mK resolution fixed to the exterior of the cell, close to one of its end. The probe was calibrated on site by comparison with two reference temperature probes that had been regularly calibrated by the BIPM thermometry service, providing a calibration uncertainty of 0.018 K. The cell was placed together with the photodiode within an enclosure in black Plexiglas to avoid stray light and also to stabilize the temperature, which was typically 295 K with less than 0.3 K variations during the measurement series. In order to measure temperature inhomogeneities in the cell, a separate series of measurements were performed, prior to the absorption measurements, with an additional probe installed inside the cell at its center. Ozone evaporation-condensation cycles were performed so as to detect any temperature difference between the inside and outside of the cell, or between the center and the cell end. A maximum difference of 0.045 K was measured, from which an uncertainty component $u_{dT} = 0.026$ K was deduced. The probe inside the cell was then removed for absorption measurements to avoid ozone dissociation caused by the probe itself.

3.4 Optical path length

As explained in Sect. 2.3.1 the absorption cell path length was measured by interferometry. Uncertainties attached to all parameters required during this measurement were evaluated and are summarized in Table 1. The main uncertainty component was the number of fringes counted with the setup, which consisted of an electronic voltmeter to record the fringes signal from the photodiode on which interferences were created. The number of fringes was further counted with a program developed specifically for this purpose and double checked directly. Through this process it was possible to determine

AMTD
7, 8067–8100, 2014

where the fringe pattern started and ended with an accuracy of one eighth of a fringe precision, resulting in a standard uncertainty of 0.048 fringes, assuming a rectangular distribution.

A series of twenty independent measurements were performed, resulting in an average cell length of 48.33 mm with a standard deviation of 0.02 mm. In addition, the possibility of a slight misalignment of the laser beam was taken into account. The beam alignment was performed using two diaphragms placed before and after the cell and kept in place with a 3 mm diameter aperture. Considering the 3° angled windows and a cell length of 48.33 mm, the shortest straight optical path hitting the diaphragm openings is

$$L_{\min} = \sqrt{(3)^2 + (48.33 - 3\tan 3)^2} = 48.27\,\text{mm} \quad (6)$$

and the longest straight optical path is

$$L_{\max} = \sqrt{(3)^2 + (48.33 + 3\tan 3)^2} = 48.58\,\text{mm} \quad (7)$$

Assuming that any possible straight optical length in between these two lengths is equally possible, the standard uncertainty on the average cell length is (48.58-48.27)/(2$\sqrt{3}\sqrt{2}$) = 0.09 mm, to be further combined with the uncertainty on the cell length as deduced from the interferometric measurements, resulting in a standard combined uncertainty of 0.11 mm.

3.5 Absorbance

The electronic measurement system is described in Petersen et al. (2012). The intensity stabilization was ensured by the AOM, leading to a transmittance I/I_0 with a relative stability better than 10^{-4} on the control light trap LT1 and better than 3×10^{-4} on the measurement light trap LT2. No further normalization of the light intensity was required. A relative uncertainty of 3×10^{-4} on the transmittance, resulting in a relative uncertainty $u_R(A_e) = 3.5 \times 10^{-4}$ on the absorbance A_e, was therefore considered.

AMTD
7, 8067–8100, 2014

3.6 Uncertainty budget

Table 2 lists the sources of uncertainty in one typical measurement at a mean sample pressure of 0.5 mbar. The four components in Table 2 can be considered as uncertainties due to systematic effects. The main contribution comes from the uncertainty on the ozone fraction that represents about 60 % of the total uncertainty. The relative uncertainty resulting from these calculations has a very minor dependency on the sample pressure, with a maximum value of 0.291 % of the cross-section value at the lowest end of the pressure range (0.2 mbar) and a minimum value of 0.289 % at the highest end of the range (1 mbar). A constant relative uncertainty $u_R(\sigma) = 0.29$ % was thus considered for the entire range.

4 Ozone absorption cross-section values at the three laser wavelengths

Three series of measurements, i.e. nine points at different pressures covering the range 0.2 mbar to 1 mbar were performed at the three laser wavelengths: 244.06 nm, 248.32 nm and 257.34 nm. The average values are reported in Table 3. With the expanded uncertainty calculated as explained previously. A new value at the 253.65 nm line of mercury is also included in the same table, with the calculations performed to obtain it further explained in the next section.

To compare the results obtained here with previously published data, the dataset from Bogumil (Bogumil et al., 2003) was chosen as the best representative historical conventional values used for ozone absorption cross sections. This is because this group performed relative measurements using the absorption of ozone at 253.65 nm together with the cross-section measured by Hearn (1961) to deduce the concentrations in its measurements. The values published here, together with the values derived from measurements by Gorshelev et al. (2014), Brion et al. (1998) and Burrows et al. (1999) are compared as a difference from those of Bogumil. The Bogumil values here are only

AMTD
7, 8067–8100, 2014

used for comparison purposes, therefore they are considered as conventional with no uncertainty. The results are plotted in Fig. 6.

When analysing the data plotted in Fig. 6, it is important to bear in mind that Burrows et al. (1999) and Bogumil et al. (2003) both performed measurements scaled to the reference value of Hearn measured at 253.65 nm. By comparison, Gorshelev et al. (2014) and Brion et al. (1998) implemented the same principle as the work reported in this paper, in which the ozone concentration is assessed independently by the measurement of the pressure of a pure sample. The two groups are clearly distinct on the plot.

Figure 6 also demonstrates that smaller uncertainties can be reached by the second method. This is however not exact, as the uncertainties associated with measurements relative to a reference are strongly dependent on the uncertainty on the reference, as already reported in Petersen et al. (2012). Therefore relative measurements would also benefit from using a reference with a reduced uncertainty compared to the Hearn value.

5 Ozone absorption cross-section at the mercury lamp wavelength for surface ozone measurements

The conventional reference value implemented for surface ozone measurements based on absorption at the 253.65 nm line of mercury is the value measured by Hearn in 1961, and is equal to 11.476×10^{-18} cm^2 molecule^{-1} (Hearn, 1961), with a relative expanded uncertainty of 2.12 % (Viallon et al., 2006b). The methodology used to calculate absorption cross sections at different wavelengths as reported previously (Petersen et al., 2012), was used to calculate three values of the ozone absorption cross-section at the mercury wavelength used in the SRP. The three calculated values are 11.27×10^{-18} cm^2 molecule^{-1}, 11.30×10^{-18} cm^2 molecule^{-1} and 11.25×10^{-18} cm^2 molecule^{-1} using comparisons performed at the respective laser wavelengths of 244.06 nm, 248.32 nm and 257.34 nm, resulting in an average value of 11.27×10^{-18} cm^2 molecule^{-1} with a relative standard deviation of the mean of 0.17 %.

AMTD
7, 8067–8100, 2014

These results show a good agreement with the three series of measurements, which result in a negligible reproducibility uncertainty compared with our measurement uncertainty of 0.35 %. The uncertainty of the SRP without the ozone cross-section component is equal to 0.3 %, the main contributor being the path length uncertainty equal to $2.89 \times 10^{-3} x(O_3)$, which takes into account reflections of light on the absorption cell windows and the non-collimated beam shape, as explained by Viallon et al. (2006b). Since this publication, the gas cells in SRPs maintained at the BIPM have been replaced with cells in quartz with their windows tilted by a 3° angle, following the improvements recommended by Norris et al. (2013). Although there are indications that reflections of light are now avoided, this uncertainty component has not yet been re-evaluated. With the current SRP uncertainty budget, we obtain a relative standard uncertainty of 0.46 % on the ozone cross-section value at 253.65 nm.

The cross-section value at the mercury wavelength calculated above is 1.8 % lower than the reference value of Hearn. If this new value was to be used in SRPs, it would mean an average increase of the measured ozone concentration of 1.8 %. This is consistent with the results obtained for gas phase titration in the international comparison CCQM-P28 during which the bias between both methods was observed. The BIPM is working on reducing uncertainties for this method and this will be the subject of a future publication.

6 Conclusions

An experimental setup was developed to generate ozone samples of high purity and to carefully evaluate their purity to obtain an accurate basis for measurements of ozone absorption cross-sections with a laser in the Hartley band.

The use of an in-house cryogenic ozone generator together with a method based on cycles of evaporation and condensation of ozone led to gaseous samples with purity better than 98.9 %. Two analytical techniques, RGA and FTIR, were further

AMTD
7, 8067–8100, 2014

implemented to confirm this value and to show that oxygen was the main impurity present in the samples, due to the reaction of ozone with surfaces.

This study reports absorption measurements performed for the first time in the Hartley band using a laser as the light source, allowing enhanced intensity stability together with an accurate knowledge of the absorption path length. Accurate values of the ozone cross-section at three wavelengths 244.06 nm, 248.32 nm and 257.34 nm could be measured with a relative expanded uncertainty better than 0.7 %. Compared to published data at the same wavelengths, the results obtained in this work are in good agreement with other recent values, and have the advantage of being reported with smaller uncertainties, and show the same level of bias with historical data sets.

Based on comparisons with a Standard Reference Photometer equipped with a mercury lamp as the light source, a mean value of 11.27×10^{-18} cm^2 molecule^{-1} was deduced for the ozone cross-section at the 253.65 nm line of mercury, with an expanded relative uncertainty of 0.92 %. This value is 1.8 % lower than the value measured by Hearn and is in closer agreement with measurements based on the gas phase titration of ozone with nitrogen monoxide as will be presented in a future publication.

Acknowledgements. The authors would like to acknowledge the contributions of Edgar Flores (BIPM) in the FTIR analysis and Lennart Robertsson (BIPM) in the absorption cell path length measurement. All data used to deduce the ozone cross-sections were acquired experimentally and saved in ASCII format files. All files will be kept at the BIPM and can be communicated on demand. Data not acquired at the BIPM are published values of the ozone cross-section and in that case the sources are cited in this paper.

References

Anderson, S. and Mauersberger, K.: Calibration of a mass spectrometer experiment for ozone, Rev. Sci. Instrum., 52, 1025–1028, 1981.

Bass, A. M. and Paur, R. J.: The ultraviolet cross-section of ozone I: measurements, in: Quadriennial Ozone Symposium, Halkidiki, Greece, 606–616, 1984.

AMTD

7, 8067–8100, 2014

BIPM, CEI, FICC, ISO, OIML, UICPA, and UIPPA: Guide to the Expression of Uncertainty in Measurement, International Organization for Standardization, Geneva, 101 pp., 1995.

Birch, K. P. and Downs, M. J.: An updated Edlen equation for the refractive index of air, Metrologia, 30, 155–162, doi:10.1088/0026-1394/30/3/004, 1993.

Bogumil, K., Orphal, J., Homann, T., Voigt, S., Spietz, P., Fleischmann, O. C., Vogel, A., Hartmann, M., Kromminga, H., Bovensmann, H., Frerick, J., and Burrows, J. P.: Measurements of molecular absorption spectra with the SCIAMACHY pre-flight model: instrument characterization and reference data for atmospheric remote-sensing in the 230–2380 nm region, J. Photoch. Photobio. A, 157, 167–184, 2003.

Brion, J., Coquart, B., Daumont, D., Jenouvrier, A., Malicet, J., and Merienne, M. F.: High resolution laboratory absorption cross sections of ozone and nitrogen dioxide, photo-oxid., precursors prod., in: Proc. EUROTRAC Symp. '92, 2nd, 423–426, 1993.

Brion, J., Chakir, A., Charbonnier, J., Daumont, D., Parisse, C., and Malicet, J.: Absorption spectra measurements for the ozone molecule in the 350–830 nm region, J. Atmos. Chem., 30, 291–299, 1998.

Burrows, J. P., Richter, A., Dehn, A., Deters, B., Himmelmann, S., Voigt, S., and Orphal, J.: Atmospheric remote-sensing reference data from GOME: 2. Temperature-depedent absorption cross-sections of O_3 in the 231–794 nm range, J. Quant. Spectrosc. Ra., 61, 509–517, 1999.

Castrillo, A., Gagliardi, G., Casa, G., and Gianfrani, L.: Combined interferometric and absorption-spectroscopic technique for determining molecular line strengths: applications to CO_2, Phys. Rev. A, 67, 062503–062501, 2003.

Daudé, B., Elandaloussi, H., and Janssen, C.: On the gas dependence of thermal transpiration and a critical appraisal of correction methods for capacitive diaphragm gauges, Vacuum, 104, 77–87, doi:10.1016/j.vacuum.2014.01.002, 2013.

Galbally, I. E., Schultz, M. G., Buchmann, B., Gilge, S., Guenther, F. R., Koide, H., Oltmans, S., Patrick, L., Sheel, H. E., Smit, H., Steinbacher, M., Steinbrecht, W., Tarasowa, O., Viallon, J., Voltz-Thomas, A., Weber, M., Wielgosz, R. I., and Zellweger, C.: Guidelines for Continuous Measurements of Ozone in the Troposphere, World Meteorological Organization, Geneva, 2013.

Gorshelev, V., Serdyuchenko, A., Weber, M., Chehade, W., and Burrows, J. P.: High spectral resolution ozone absorption cross-sections – Part 1: Measurements, data analysis and

AMTD
7, 8067–8100, 2014

comparison with previous measurements around 293 K, Atmos. Meas. Tech., 7, 609–624, doi:10.5194/amt-7-609-2014, 2014.
Hearn, A. G.: The absorption of ozone in the ultra-violet and visible regions of the spectrum, P. Phys. Soc., 78, 932–940, 1961.
ISO: Ambient Air – Determination of Ozone – Ultraviolet Photometric Method, International Organization for Standardization, 1996.
Janssen, C., Simone, D., and Guinet, M.: Preparation and accurate measurement of pure ozone, Rev. Sci. Instrum., 82, 034102, doi:10.1063/1.3557512, 2011.
Klausen, J., Zellweger, C., Buchmann, B., and Hofer, P.: Uncertainty and bias of surface ozone measurements at selected Global Atmosphere Watch sites, J. Geophys. Res.-Atmos., 108, 4622, doi:10.1029/2003JD003710, 2003.
Malicet, J., Daumont, D., Charbonnier, J., Parisse, C., Chakir, A., and Brion, J.: Ozone UV spectroscopy. II. Absorption cross-sections and temperature dependence, J. Atmos. Chem., 21, 263–273, 1995.
Mauersberger, K., Hanson, D., and Morton, J.: A new ozone standard: the vapor pressure of ozone at liquid argon temperatures, Geophys. Res. Lett., 12, 89–92, 1985.
Mauersberger, K., Barnes, J., Hanson, D., and Morton, J.: Measurement of the ozone absorption cross-section at the 253.7 nm mercury line, Geophys. Res. Lett., 13, 671–673, 1986.
Mauersberger, K., Hanson, D., Barnes, J., and Morton, J.: Ozone vapor pressure and absorption cross-section measurements: introduction of an ozone standard, J. Geophy. Res. D, 92, 8480–8482, 1987.
Norris, J. E., Choquette, S. J., Viallon, J., Moussay, P., Wielgosz, R., and Guenther, F. R.: Temperature measurement and optical path-length bias improvement modifications to National Institute of Standards and Technology ozone reference standards, J. Air Waste Manage., 63, 565–574, doi:10.1080/10962247.2013.773951, 2013.
Orphal, J.: A Critical Review of the Absorption Cross-Sections of O_3 and NO_2 in the 240–790 nm Region, ESA Technical Note MO-TN-ESA-GO-0302, European Space Agency, Noordwijk, 2002.
Petersen, M., Viallon, J., Moussay, P., and Wielgosz, R. I.: Relative measurements of ozone absorption cross-sections at three wavelengths in the Hartley band using a well-defined UV laser beam, J. Geophys. Res.-Atmos., 117, D05301, doi:10.1029/2011jd016374, 2012.

AMTD
7, 8067–8100, 2014

Serdyuchenko, A., Gorshelev, V., Weber, M., Chehade, W., and Burrows, J. P.: High spectral resolution ozone absorption cross-sections – Part 2: Temperature dependence, Atmos. Meas. Tech., 7, 625–636, doi:10.5194/amt-7-625-2014, 2014.

Tanimoto, H., Mukai, H., Hashimoto, S., and Norris, J. E.: Intercomparison of ultraviolet photometry and gas-phase titration techniques for ozone reference standards at ambient levels, J. Geophys. Res.-Atmos., 111, D16313, doi:10.1029/2005JD006983, 2006.

Viallon, J., Moussay, P., Esler, M., Wielgosz, R., Bremser, W., Novák, J., Vokoun, M., Botha, A., Janse Van Rensburg, M., Zellweger, C., Goldthorp, S., Borowiak, A., Lagler, F., Walden, J., Malgeri, E., Sassi, M. P., Morillo Gomez, P., Fernandez Patier, R., Galan Madruga, D., Woo, J.-C., Doo Kim, Y., Macé, T., Sutour, C., Surget, A., Niederhauser, B., Schwaller, D., Frigy, B., Györgyné Váraljai, I., Hashimoto, S., Mukai, H., Tanimoto, H., Ahleson, H. P., Egeløv, A., Ladegard, N., Marsteen, L., Tørnkvist, K., Guenther, F. R., Norris, J. E., Hafkenscheid, T. L., Van Rijn, M. M., Quincey, P., Sweeney, B., Langer, S., Magnusson, B., Bastian, J., Stummer, V., Fröhlich, M., Wolf, A., Konopelko, L. A., Kustikov, Y. A., and Rumyanstev, D. V.: Pilot study: International comparison CCQM-P28: ozone at ambient level, Metrologia, Tech. Suppl., 43, 08010, doi:10.1088/0026-1394/43/1A/08010, 2006a.

Viallon, J., Moussay, P., Norris, J. E., Guenther, F. R., and Wielgosz, R. I.: A study of systematic biases and measurement uncertainties in ozone mole fraction measurements with the NIST Standard Reference Photometer, Metrologia, 43, 441–450, 2006b.

AMTD
7, 8067–8100, 2014

Table 1. Uncertainty budget for the absorption cell light path length measurement.

Parameter	Typical value	Standard uncertainty
Number of fringes F	41.35	0.048
Temperature T	22.72 °C	0.034 °C
Pressure P_a	1018.84 hPa	0.945 Pa
Wavelength in air λ_a	0.632827 µm	3.47×10^{-6} µm
Wavelength in vacuum λ_v	0.632991 µm	0.29×10^{-6} µm
L_{opt}	48.32 mm	0.06 mm

AMTD
7, 8067–8100, 2014

Table 2. Systematic and statistical sources of uncertainties, indicated here for one typical measurement of the ozone absorption cross-section at a sample pressure of 0.51 mbar and a laser wavelength of 244.06 nm.

Parameter	Typical value	Relative uncertainty
Sample pressure P_T	0.51 mbar	1×10^{-3}
Ozone fraction x	0.9918 mol mol^{-1}	2×10^{-3}
Temperature T	295.65 K	9×10^{-5}
Optical length L_{opt}	48.33 mm	2×10^{-3}
Absorbance A_e	0.564	6.0×10^{-5}
Cross-section systematic relative uncertainty		2.90×10^{-3}
Linear regression relative uncertainty		1.5×10^{-3}
Reproducibility (standard deviation of the mean)		3.7×10^{-4}
Combined expanded relative uncertainty		6.5×10^{-3}

AMTD
7, 8067–8100, 2014

Table 3. Values of the ozone absorption cross-section at the three wavelengths of the argon-ion laser and their expanded uncertainties (coverage factor 95 %).

Laser wavelength in vacuum [*air*] (and expanded uncertainty) / nm	Ozone absorption cross-section (and expanded uncertainty) / (10^{-18} cm^2 molecule^{-1})
244.062 [*243.998*] (0.001)	9.48 (0.06)
248.323 [*248.249*] (0.001)	10.44 (0.07)
257.337 [*257.260*] (0.001)	11.07 (0.07)
253.73 [*253.65*] line of mercury	11.27 (0.09)

AMTD
7, 8067–8100, 2014

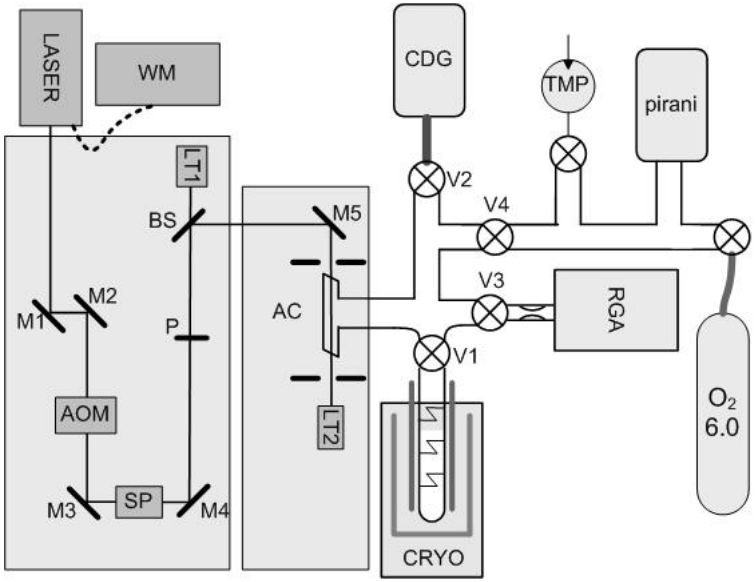

Figure 1. Measurement setup. AOM – Accousto-Optic Modulator; BS – Beam Splitter; CDG – Capacitive Diaphragm Gauge (Baratron); CRYO – cryogenic ozone generator; LT – Light Trap; M – Mirror; RGA – Residual Gas Analyser (Quadrupole mass spectrometer); TMP – Turbo Molecular Pump; V – Valve; WM – Wavemeter.

AMTD
7, 8067–8100, 2014

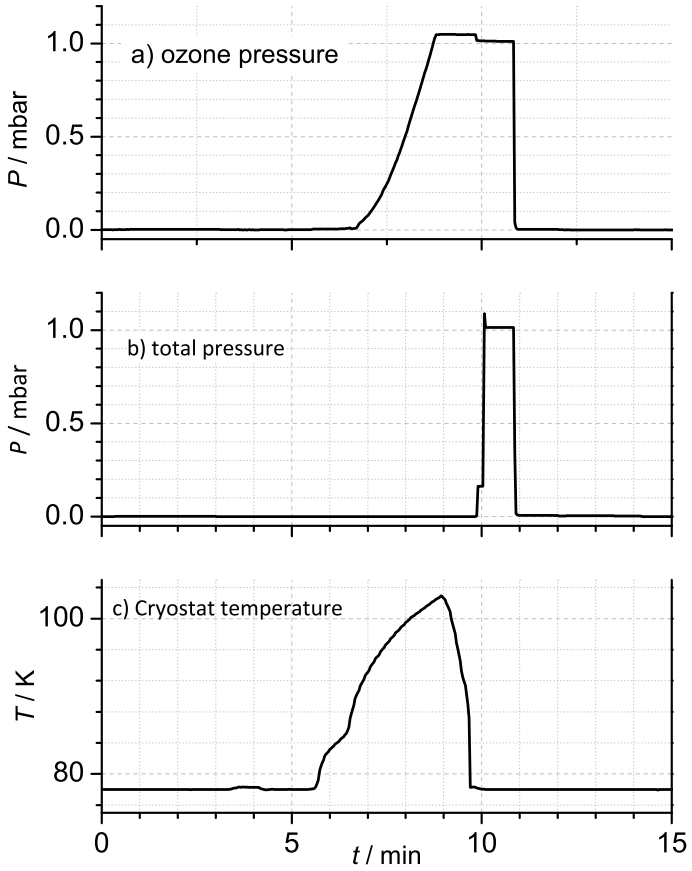

Figure 2. The measured values of key parameters during a typical evaporation-condensation cycle: **(a)** Ozone partial pressure deduced from the absorption measurement $P(O_3)$, **(b)** total pressure P_T measured with the Baratron gauge and **(c)** temperature T_{cryo} inside the cryostat.

AMTD
7, 8067–8100, 2014

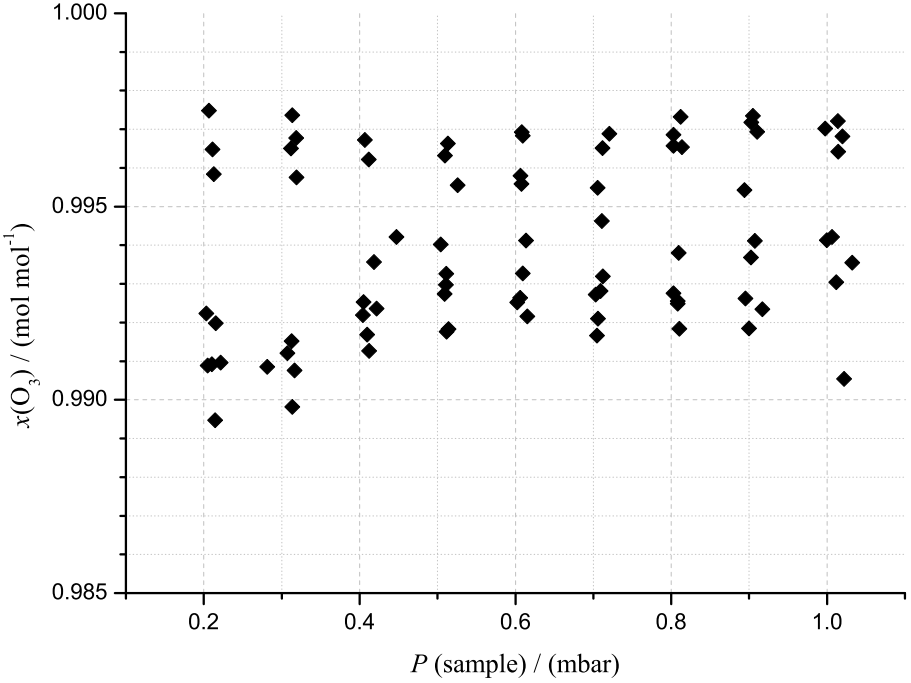

Figure 3. Ozone mole fractions $x(O_3)$ in mol mol^{-1} calculated for all measurement points, plotted vs. the sample pressure P_T in mbar.

AMTD
7, 8067–8100, 2014

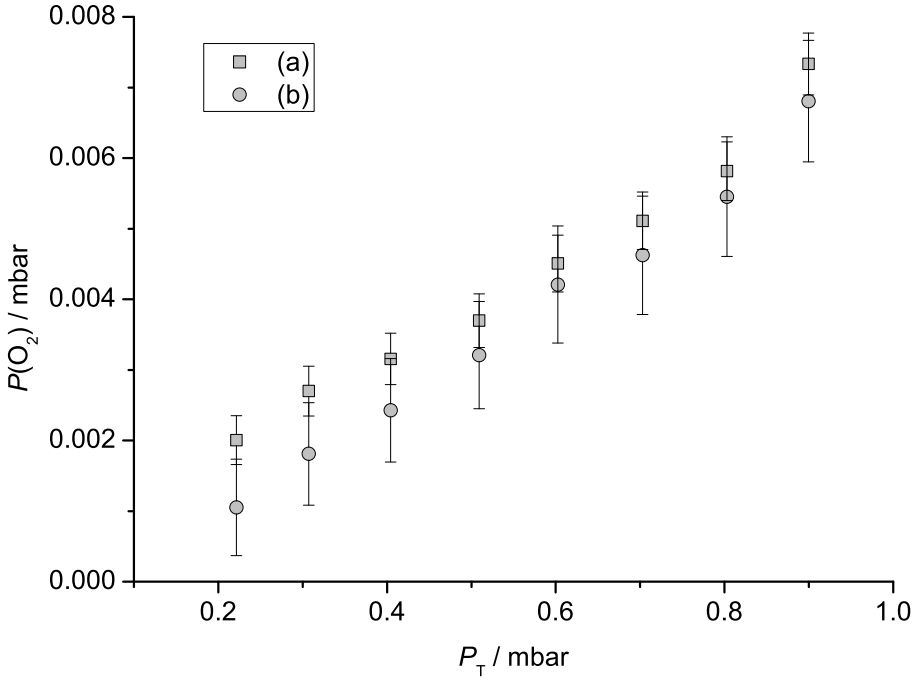

Figure 4. Oxygen pressure in the residual gas evaluated by pressure difference **(a)** and with the calibrated RGA **(b)**.

AMTD
7, 8067–8100, 2014

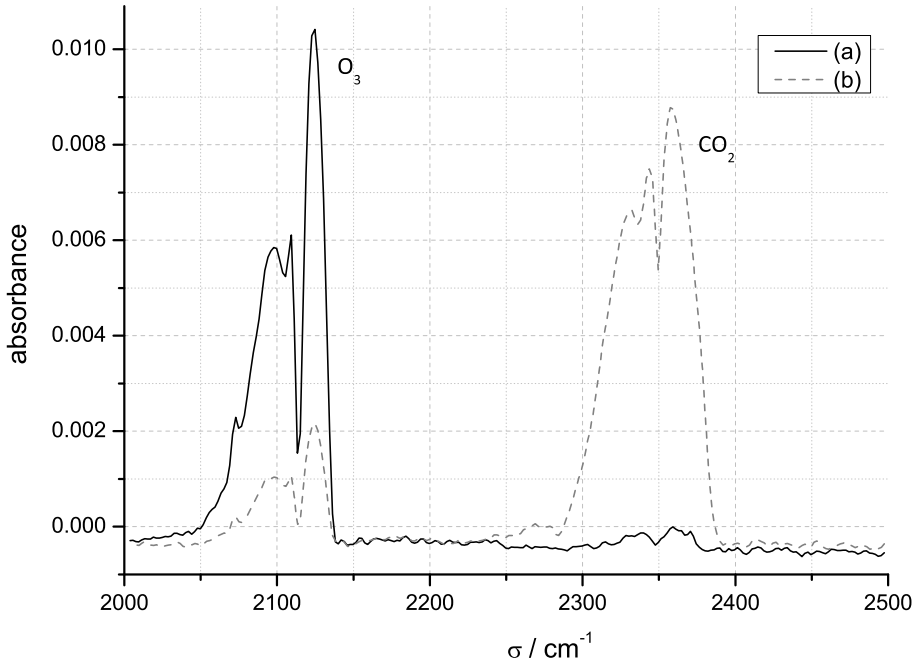

Figure 5. FTIR absorbance spectra recorded on a gaseous ozone sample at 3 mbar **(a)** and on the same sample after 12 h in the FTIR cell **(b)**. Absorption peaks of ozone and carbon dioxide are indicated.

AMTD
7, 8067–8100, 2014

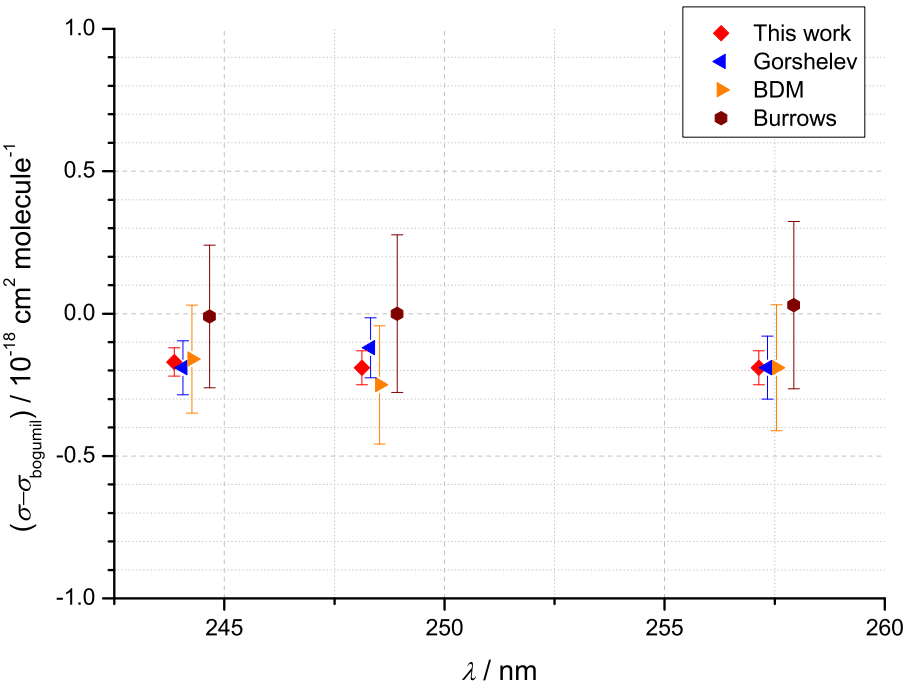

Figure 6. Comparison between the ozone absorption cross-section values measured by different groups at the three laser wavelengths examined in this study. Data were taken from the recent publication of Gorshelev et al. (2014) and the values measured by Bogumil are subtracted from the other values. Wavelengths are plotted with a 0.2 nm shift from each other for clarity.

AMTD
7, 8067–8100, 2014